Inverse kinematics of the 2-RRS-1-RRRR cable actuated mechanism

Isaac John[0000−0001−5803−9862] and
Santhakumar Mohan[0000−0002−4741−0379] and
Philippe Wenger[0000−0002−6608−4484]

Abstract This work presents an inverse kinematics (IK) formulation of a spatial, cable actuated 2-degree-of-freedom mechanism. The 2-RRS-1-RRRR mechanism studied in this work is derived from the well-known quaternion joint. The system of 13 constraint equations have mixed variables in joint and task spaces, and is solved using polynomial homotopy continuation. Further on, the extraneous solutions are eliminated using the filtering conditions.

1 Introduction

Cable-actuated parallel mechanisms (CAPMs) can be considered bioinspired solutions that mimic the functions of vertebral columns. These mechanisms can be used in applications where a rigid manipulator is too stiff for safe interactions with the environment, and a soft robot lacks the necessary minimum payload capacity. The variable stiffness capabilities of CAPMs make them inherently safer for interactions with their surroundings. The central parallel mechanism that is manipulated by the peripheral cables provides the required minimum stiffness, making it more suitable than compliant soft robots for precise payload manipulation [9].

A recent well-known example, called the Quaternion (Q) joint [5], has been adopted in a wide variety of applications [6, 3]. However, the Q joint is theoretically a zero-mobility mechanism, with an instantaneous mobility of two in its zero-orientation configuration [5]. The Q joint can be regarded as a spatial realisation of the planar antiparallelogram X mechanism, whose output link exhibits a motion

Isaac John and Santhakumar Mohan
Indian Institute of Technology Palakkad, 678623 Kerala, India, e-mail: 132114001@smail.iitpkd.ac.in (Isaac John), e-mail: santhakumar@iitpkd.ac.in (Santhakumar Mohan)

Philippe Wenger
Nantes Universite, Ecole Centrale de Nantes, CNRS, LS2N, 44000 Nantes, France e-mail: Philippe.Wenger@ls2n.fr

equivalent to an ellipse rolling over a fixed ellipse. For specific link dimensions, the ellipse rolling motion can closely approximate a motion equivalent to a circle rolling over a fixed circle. When these dimensions are applied to the spatial Q joint, it has been observed that if the error between the true ellipse rolling motion and the approximated circle rolling motion is small enough to be absorbed within the link flexures and joint clearances, the Q joint can exhibit a practical mobility of two [5, 6]. In all of the above applications, the link lengths are chosen so that the mechanism closely approximates a spherical rolling motion. This approximation simplifies the kinematic model, as the distance between the centres of the base and top platforms is considered constant.

Muralidharan et al. [7, 8] proposed an elaborate framework for the optimal design of planar cable-actuated X joints and cable-actuated variable stiffness manipulators, which are designed by serially stacking X joints, with link dimensions included among the design variables. Due to the specific requirements for the link lengths of Q joints, a similar optimal design investigation would not be possible. As a result, we proposed a cable-actuated 2-RRS-1-RRRR (R-revolute, S-spherical) joint as an alternative to the Q joint in our previous works [4]. This mechanism exhibits a global mobility of two, regardless of its link dimensions. In this work, we formulate the inverse kinematics model of the 2-RRS-1-RRRR mechanism, where the possible configurations for a pair of independent task-space coordinates are investigated.

2 Description of the mechanism

The base and top platforms of radius r (with centrally mounted frames of references {B} and {P}) are constrained by an RRRR limb and two RRS limbs. The RRRR limb is attached to the base (resp. top) platform at a radial coordinate of $(r,\ 90^\circ)$ (resp. $(r,\ 270^\circ)$) with respect to X_B (resp. X_P) axis. The two RRS limbs are attached to the base (resp. top) at radial coordinates $(r,\ 210^\circ)$ and $(r,\ 330^\circ)$ (resp. $(r,\ 30^\circ)$ and $(r,\ 150^\circ)$) with respect to X_B (resp. X_P) axis. As depicted in Fig. 1, the local frames {a}, {b}, and {c} are attached to the proximal ends of limbs 1 (RRRR), 2, and 3 (RRS). Similarly, three frames {d}, {e}, and {f} are attached to the distal ends of the three limbs. The DH parameters associated with all three limbs are presented in Tables 1-3. Not all frames from the DH tables are shown in Fig. 1 to avoid overcluttering. There is an offset h_1 between the first two R joints (R $\perp$ R) at the proximal ends of all three limbs. The offset between the two R joints (R $\perp$ R) at the distal end of limb 1 is denoted as h_2. The link length between the 2$^{\text{nd}}$ and 3$^{\text{rd}}$ R joints (R $\parallel$ R) of limb 1, and between the 2$^{\text{nd}}$ R joint and the S joint of limbs 2 and 3, is l. The mechanism is actuated by 3 cables anchored to the base and top platforms at radial coordinates $(r',\ 90^\circ)$, $(r',\ 210^\circ)$, and $(r', 330^\circ)$, respectively, with respect to the X_B and X_P axes, as shown in Fig.1..

The pose of platform frame {P} w.r.t. the base frame {B} is expressed in terms of six task-space coordinates: three position coordinates p_x, p_y, p_z and X-Y-Z Euler angles θ, ψ, and ϕ. The base-to-platform transformation matrix is thus:

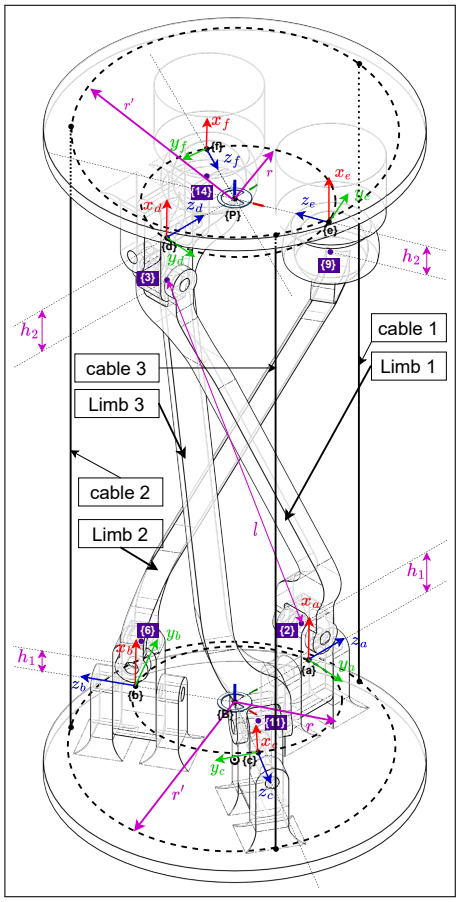

Fig. 1: The 2-RRS-1-RRRR mechanism.

Table 1: DH parameter table for limb 1 (RRRR).

Transformation	α_{i-1}	a_{i-1}	θ_i	d_i
${}^{a}T_1$	0	0	θ_1	0
${}^{1}T_2$	$\frac{\pi}{2}$	h_1	θ_2	0
${}^{2}T_3$	0	l	θ_3	0
${}^{3}T_d$	$\frac{-\pi}{2}$	h_2	θ_4	0

Table 2: DH parameters for limb 2 (RRS).

Transformation	α_{i-1}	a_{i-1}	θ_i	d_i
${}^{b}T_5$	0	0	θ_5	0
${}^{5}T_6$	$\frac{\pi}{2}$	h_1	θ_6	0
${}^{6}T_7$	0	l	θ_7	0
${}^{7}T_8$	$-\frac{\pi}{2}$	0	$\theta_8 - \frac{\pi}{2}$	0
${}^{8}T_9$	$-\frac{\pi}{2}$	0	θ_9	0

Table 3: DH parameters for limb 3 (RRS).

Transformation	α_{i-1}	a_{i-1}	θ_i	d_i
${}^{c}T_{10}$	0	0	θ_{10}	0
${}^{10}T_{11}$	$\frac{\pi}{2}$	h_1	θ_{11}	0
${}^{11}T_{12}$	0	l	θ_{12}	0
${}^{12}T_{13}$	$-\frac{\pi}{2}$	0	$\theta_{13} - \frac{\pi}{2}$	0
${}^{13}T_{14}$	$-\frac{\pi}{2}$	0	θ_{14}	0

$$
{}^{\mathrm{B}}\mathbf{T}_{\mathrm{P}} = \begin{bmatrix} C_\phi C_\psi & -C_\psi S_\phi & S_\psi & p_x \\ C_\theta S_\phi + C_\phi S_\theta S_\psi & C_\theta C_\phi - S_\theta S_\phi S_\psi & -C_\psi S_\theta & p_y \\ S_\theta S_\phi - C_\theta C_\phi S_\psi & C_\phi S_\theta + C_\theta S_\phi S_\psi & C_\theta C_\psi & p_z \\ 0 & 0 & 0 & 1 \end{bmatrix} \tag{1}
$$

where $C_k = \cos(k)$ and $S_k = \sin(k),\ k = \phi,\ \psi,\ \theta$

As the mechanism has two degrees of freedom (d.o.f.), only two variables in the task-space, (θ, ψ), are considered independent, while the remaining four are solved using the loop-closure constraints described in the remainder of this paper. In the following, the IK problem is solved, namely, the 3 cable lengths are determined for a given pose of the platform.

3 Formulating the constraint equations

Referring to Fig. 1, the loop-closure constraints can be described as follows:

1. The distance between frames {2} and {3} of limb 1 is l.
2. The distance between frames {6} and {9} of limb 2 is l.
3. The distance between frames {11} and {14} of limb 3 is l.
4. The origins of frames {B}, {a}, {2}, {3}, {d}, and {P} all lie on a plane.

The above-mentioned constraints can be mathematically represented as:

$$\text{Constraint 1} \implies \left({}^{\mathrm{a}}\mathbf{p}_3 - {}^{\mathrm{a}}\mathbf{p}_2\right)^{\mathrm{T}}\left({}^{\mathrm{a}}\mathbf{p}_3 - {}^{\mathrm{a}}\mathbf{p}_2\right) - l^2 = 0 \tag{2a}$$

$$\text{Constraint 2} \implies \left({}^{\mathrm{b}}\mathbf{p}_9 - {}^{\mathrm{b}}\mathbf{p}_6\right)^{\mathrm{T}}\left({}^{\mathrm{b}}\mathbf{p}_9 - {}^{\mathrm{b}}\mathbf{p}_6\right) - l^2 = 0 \tag{2b}$$

$$\text{Constraint 3} \implies \left({}^{\mathrm{c}}\mathbf{p}_{14} - {}^{\mathrm{c}}\mathbf{p}_{11}\right)^{\mathrm{T}}\left({}^{\mathrm{c}}\mathbf{p}_{14} - {}^{\mathrm{c}}\mathbf{p}_{11}\right) - l^2 = 0 \tag{2c}$$

$$\text{Constraint 4} \implies \left({}^{\mathrm{B}}\mathbf{p}_{\mathrm{a}} \times {}^{\mathrm{B}}\mathbf{p}_{\mathrm{d}}\right) \cdot \left[p_x \; p_y \; p_z\right]^{\mathrm{T}} = 0 \tag{2d}$$

where $\left[{}^{\mathrm{a}}\mathbf{p}_2^{\mathrm{T}}\ 1\right]^{\mathrm{T}} = {}^{\mathrm{a}}\mathbf{T}_1 \times {}^{1}\mathbf{T}_2 \times [0\,0\,0\,1]^{\mathrm{T}}$, $\left[{}^{\mathrm{a}}\mathbf{p}_3^{\mathrm{T}}\ 1\right]^{\mathrm{T}} = \left({}^{\mathrm{B}}\mathbf{T}_{\mathrm{a}}\right)^{-1} \times {}^{\mathrm{B}}\mathbf{T}_{\mathrm{P}} \times \left({}^{3}\mathbf{T}_{\mathrm{d}} \times {}^{\mathrm{d}}\mathbf{T}_{\mathrm{P}}\right)^{-1} \times [0\,0\,0\,1]^{\mathrm{T}}$, $\left[{}^{\mathrm{b}}\mathbf{p}_6^{\mathrm{T}}\ 1\right]^{\mathrm{T}} = {}^{\mathrm{b}}\mathbf{T}_5 \times {}^{5}\mathbf{T}_6 \times [0\,0\,0\,1]^{\mathrm{T}}$, $\left[{}^{\mathrm{b}}\mathbf{T}_9\ 1\right]^{\mathrm{T}} = \left({}^{\mathrm{B}}\mathbf{T}_{b}\right)^{-1} \times {}^{\mathrm{B}}\mathbf{T}_{\mathrm{P}} \times \left({}^{9}\mathbf{T}_{\mathrm{e}} \times {}^{\mathrm{e}}\mathbf{T}_{\mathrm{P}}\right)^{-1} \times [0\,0\,0\,1]^{\mathrm{T}}$, $\left[{}^{\mathrm{c}}\mathbf{p}_{11}^{\mathrm{T}}\ 1\right]^{\mathrm{T}} = {}^{\mathrm{c}}\mathbf{T}_{10} \times {}^{10}\mathbf{T}_{11} \times [0\,0\,0\,1]^{\mathrm{T}}$, $\left[{}^{\mathrm{c}}\mathbf{p}_{14}^{\mathrm{T}}\ 1\right]^{\mathrm{T}} = \left({}^{\mathrm{B}}\mathbf{T}_{c}\right)^{-1} \times {}^{\mathrm{B}}\mathbf{T}_{\mathrm{P}} \times \left({}^{14}\mathbf{T}_{\mathrm{f}} \times {}^{\mathrm{f}}\mathbf{T}_{\mathrm{P}}\right)^{-1} \times [0\,0\,0\,1]^{\mathrm{T}}$. The transformation matrices from the base frame {B} to the limb local frames {a}, {b}, and {c} are trivial. The same applies to the transformations between the distal frames of the limbs: {d}, {e}, and {f} to the platform frame {P}. To preserve the trigonometric identities of the task-space variable ϕ, the following algebraic constraint is also appended to the constraint Eqs. 2.

$$S_\phi^2 + C_\phi^2 - 1 = 0 \tag{3}$$

The five constraint equations Eqs. 2a–3 are polynomial equations in the variables p_x, p_y, p_z, C_ϕ, S_ϕ, $C_{\theta 1}$, $S_{\theta 1}$, $C_{\theta 4}$, $S_{\theta 4}$, $C_{\theta 5}$, $S_{\theta 5}$, $C_{\theta 10}$, and $S_{\theta 10}$, with degree 3, 2, 2, 2, and 2, respectively. Here, $C_{\theta k}$ and $S_{\theta k}$ denote $\cos(\theta_k)$ and $\sin(\theta_k)$, respectively, with $k = 1, 4, 5$, and 10. Since eight additional algebraic variables ($C_{\theta k}$ and $S_{\theta k}$, for $k = 1, 4, 5, 10$) corresponding to four joint variables are introduced in the above constraint equations, eight additional constraints are required to fully define the configuration of the mechanism for any given pair of (θ, ψ). The additional constraint equations are considered limb by limb as follows.

3.1 Additional constraint equations for limb 1

Limb 1 contributes two additional constraints. The first constraint is as follows: the origins of frames {a}, {2}, and {3} lie on a plane. This constraint can be expressed mathematically as:

$$\left({}^{\mathrm{B}}\mathbf{p}_{\mathrm{a}} \times {}^{\mathrm{B}}\mathbf{p}_2\right) \cdot {}^{\mathrm{B}}\mathbf{p}_3 = 0 \tag{4}$$

where ${}^{\mathrm{B}}\mathbf{p}_2$ and ${}^{\mathrm{B}}\mathbf{p}_3$ are respectively obtained from: $\left[{}^{\mathrm{B}}\mathbf{p}_2^{\mathrm{T}}\ 1\right]^{\mathrm{T}} = {}^{\mathrm{B}}\mathbf{T}_{\mathrm{a}} \times \left[{}^{\mathrm{a}}\mathbf{p}_2^{\mathrm{T}}\ 1\right]^{\mathrm{T}}$ and $\left[{}^{\mathrm{B}}\mathbf{p}_3^{\mathrm{T}}\ \right]^{\mathrm{T}} = {}^{\mathrm{B}}\mathbf{T}_{\mathrm{a}} \times \left[{}^{\mathrm{a}}\mathbf{p}_3^{\mathrm{T}}\ 1\right]^{\mathrm{T}}$. The position vectors ${}^{\mathrm{a}}\mathbf{p}_2$ and ${}^{\mathrm{a}}\mathbf{p}_3$ are defined at the beginning of the section. ${}^{\mathrm{B}}\mathbf{T}_{\mathrm{a}}$ is the transformation from $\{\mathrm{B}\}$ to the local limb frame $\{\mathrm{a}\}$, which is straightforward to formulate.

For the second constraint, we consider the (3,1) and (3,2) elements of the joint-space transformation matrix ${}^{\mathrm{a}}\mathbf{T}_{\mathrm{d}}^{\mathrm{js}} = {}^{\mathrm{a}}\mathbf{T}_1 \times^1 \mathbf{T}_2 \times^2 \mathbf{T}_3 \times^3 \mathbf{T}_{\mathrm{d}}$, which are given as follows:

$$\mathrm{a}\mathbf{T}_{\mathrm{d}}^{\mathrm{js}}(3,1) \quad = C_{\theta 4} \underbrace{\left(C_{\theta 3} S_{\theta 2} + C_{\theta 2} S_{\theta 3}\right)}_{K_4} \tag{5a}$$

$$\mathrm{a}\mathbf{T}_{\mathrm{d}}^{\mathrm{js}}(3,2) = S_{\theta 4} \left(- \underbrace{\left(C_{\theta 3} S_{\theta 2} + C_{\theta 2} S_{\theta 3}\right)}_{K_4} \right) \tag{5b}$$

Based on Eqs. 5, the value of K_4 in task-space can be obtained by squaring and adding the (3,1) and (3,2) elements of an equivalent transformation matrix ${}^{\mathrm{a}}\mathbf{T}_{\mathrm{d}}^{\mathrm{ts}} = \left({}^{\mathrm{B}}\mathbf{T}_{\mathrm{a}}\right)^{-1} \times {}^{\mathrm{B}}\mathbf{T}_{\mathrm{d}} \times \left({}^{\mathrm{d}}\mathbf{T}_{\mathrm{P}}\right)^{-1}$. The expression for K_4 in task space is:

$$K_4^2 = C_\psi^2 S_\theta^2 + \left(C_\phi S_\theta S_\psi + C_\theta S_\phi\right)^2 \tag{6}$$

The second additional constraint for limb 1 is obtained by equating the squared (3,1) entries of ${}^{\mathrm{a}}\mathbf{T}_{\mathrm{d}}^{\mathrm{js}}$ and ${}^{\mathrm{a}}\mathbf{T}_{\mathrm{d}}^{\mathrm{ts}}$, with K_4 substituted from Eq. 6. The resulting constraint equation is:

$$C_{\theta 4}^2 \left(C_\psi^2 S_\theta^2 + \left(C_\phi S_\theta S_\psi + C_\theta S_\phi\right)^2 \right) - C_\psi^2 S_\theta^2 = 0 \tag{7}$$

The two additional constraints on limb 1, represented by Eqs. 4 and 7, have degrees 3 and 4, respectively. To preserve the trigonometric identities between the algebraic variables $C_{\theta k}$ and $S_{\theta k}$, where $k = 1, 4$, the following two constraints, each of degree 2, are appended.

$$S_{\theta k}^2 + C_{\theta k}^2 - 1 = 0, \ k = 1, 4 \tag{8}$$

3.2 Additional constraint equations for limb 2

Limb 2 contributes one additional constraint, described as follows: The origins of frames $\{\mathrm{b}\}$, $\{6\}$, and $\{9\}$ lie on a plane. This constraint can be mathematically expressed as:

$$\left({}^{\mathrm{B}}\mathbf{p}_{\mathrm{b}} \times {}^{\mathrm{B}}\mathbf{p}_6\right) \cdot {}^{\mathrm{B}}\mathbf{p}_9 = 0 \tag{9}$$

where ${}^{\mathrm{B}}\mathbf{p}_6$ and ${}^{\mathrm{B}}\mathbf{p}_9$ are respectively obtained from: $\left[{}^{\mathrm{B}}\mathbf{p}_6^{\mathrm{T}}\ 1\right] = {}^{\mathrm{B}}\mathbf{T}_{\mathrm{b}} \times \left[{}^{\mathrm{b}}\mathbf{p}_6^{\mathrm{T}}\ 1\right]^{\mathrm{T}}$ and $\left[{}^{\mathrm{B}}\mathbf{p}_9^{\mathrm{T}}\ 1\right]^{\mathrm{T}} = {}^{\mathrm{B}}\mathbf{T}_{\mathrm{b}} \times \left[{}^{\mathrm{b}}\mathbf{p}_9^{\mathrm{T}}\ 1\right]^{\mathrm{T}}$. The position vectors ${}^{\mathrm{b}}\mathbf{p}_6$ and ${}^{\mathrm{b}}\mathbf{p}_9$ were already defined at the beginning of this section, and ${}^{\mathrm{B}}\mathbf{T}_{\mathrm{b}}$ represents the transformation from $\{\mathrm{B}\}$ to

the limb local frame {b}. The above constraint is a polynomial equation of degree 2. To preserve the trigonometric identities of the variables $C_{\theta 5}$ and $S_{\theta 5}$, the following constraint equation of degree two is appended to the already derived constraint equations.

$$C_{\theta 5}^2 + S_{\theta 5}^2 - 1 = 0 \tag{10}$$

3.3 Additional constraint equations for limb 3

The additional constraint contributed by limb 3 is similar to that of limb 2 and can be described as follows: The origins of frames {c}, {11}, and {14} lie on a plane. This constraint can be mathematically expressed as:

$$\left({}^{\mathrm{B}}\mathbf{p}_{\mathrm{c}} \times {}^{\mathrm{B}}\mathbf{p}_{11}\right) \cdot {}^{\mathrm{B}}\mathbf{p}_{14} = 0 \tag{11}$$

where ${}^{\mathrm{B}}\mathbf{p}_{11}$ and ${}^{\mathrm{B}}\mathbf{p}_{14}$ are respectively obtained from: $\left[{}^{\mathrm{B}}\mathbf{p}_{11}^{\mathrm{T}}\ 1\right] = {}^{\mathrm{B}}\mathbf{T}_{\mathrm{c}} \times \left[{}^{\mathrm{c}}\mathbf{p}_{11}^{\mathrm{T}}\ 1\right]^{\mathrm{T}}$ and $\left[{}^{\mathrm{B}}\mathbf{p}_{14}^{\mathrm{T}}\ 1\right]^{\mathrm{T}} = {}^{\mathrm{B}}\mathbf{T}_{\mathrm{c}} \times \left[{}^{\mathrm{c}}\mathbf{p}_{14}^{\mathrm{T}}\ 1\right]^{\mathrm{T}}$. The position vectors ${}^{\mathrm{c}}\mathbf{p}_{11}$ and ${}^{\mathrm{c}}\mathbf{p}_{14}$ were defined at the beginning of this section. ${}^{\mathrm{B}}\mathbf{T}_{\mathrm{c}}$ is the transformation matrix from the base frame {B} to the limb local frame {c} of the third limb. The above constraint equation is a polynomial equation of degree 2. To preserve the trigonometric identities among $C_{\theta 10}$ and $S_{\theta 10}$, the following constraint of degree two should be appended to the previously derived set of constraint equations:

$$C_{\theta 10}^2 + S_{\theta 10}^2 - 1 = 0 \tag{12}$$

4 Solving the constraint equations

The total number of constraint equations is 13. The four Eqs. 2 have degrees 3, 2, 2, and 2, respectively. The constraint Eq. 3 has a degree of 2. The additional constraints presented in Eqs. 4 and 7 have degrees 3 and 4, respectively. The two equations from Eq. 8 have degree 2 each. Eqs. 9, 10, 11, and 12 have the degrees 2 for each. Therefore, the total degree of the system of 13 polynomial equations in variables, p_x, p_y, p_z, C_ϕ, S_ϕ, $C_{\theta 1}$, $S_{\theta 1}$, $C_{\theta 4}$, $S_{\theta 4}$, $C_{\theta 5}$, $S_{\theta 5}$, $C_{\theta 10}$, $S_{\theta 10}$ is: 36,864.

For a given system of link dimensions l = 200 mm, r = 35mm, r' = 60 mm, $h_1 = h_2$ =15 mm and the independent task-space variables, the above system of constraint equations is solved using a polynomial homotopy continuation (PHC) from a Julia package [1]. For the task-space parameters $(\theta, \psi) = (-20°, -18°)$, the homotopy continuation returned 146 real solutions. However, since the constraint in Eq. 7 is squared to convert it into a polynomial equation, not all of these 146 solutions are physically realisable by the mechanism. Using the following filtering conditions to eliminate extraneous solutions, 76 feasible configurations (ignoring link interfer-

ences) are identified for the task-space variables $(\theta, \psi) = (-20°, -18°)$. The filtering conditions are as follows:

$$({}^{a}\mathbf{p}_3 - {}^{a}\mathbf{p}_2)^{\mathrm{T}} ({}^{a}\mathbf{p}_3 - {}^{a}\mathbf{p}_2) = l^2 \tag{13a}$$

$$\left({}^{b}\mathbf{p}_9 - {}^{b}\mathbf{p}_6\right)^{\mathrm{T}} \left({}^{b}\mathbf{p}_9 - {}^{b}\mathbf{p}_6\right) = l^2 \tag{13b}$$

$$({}^{c}\mathbf{p}_{14} - {}^{c}\mathbf{p}_{11})^{\mathrm{T}} ({}^{c}\mathbf{p}_{14} - {}^{c}\mathbf{p}_{11}) = l^2 \tag{13c}$$

$$(\mathbf{v}_1 \times \mathbf{v}_2) \cdot \mathbf{v}_3 = 0 \tag{13d}$$

where $\mathbf{v}_1 = {}^{a}\mathbf{p}_3 - {}^{a}\mathbf{p}_2$, $\mathbf{v}_2 = {}^{a}\mathbf{p}_{\mathrm{d}} - {}^{a}\mathbf{p}_2$, $\mathbf{v}_3 = \begin{bmatrix} p_x & p_y & p_z \end{bmatrix}^T - {}^{a}\mathbf{p}_2$.

All 76 solutions satisfying the above constraints are validated in a CAD environment, and are presented in this clickable link[1]. When considering link collisions, it appears that solution ''id 6" (see Fig.2a) is the only feasible configuration. A few additional feasible IK solutions for different platform poses $(\theta,\ \psi)$ are shown in Fig. 2.

Funding data The first author is financially supported through the Prime Minister's Research Fellowship (PMRF) scheme funded by the Ministry of Education (MoE), India

References

[1] Breiding P, Timme S (2018) HomotopyContinuation.jl: A Package for Homotopy Continuation in Julia. In: International Congress on Mathematical Software, Springer, pp 458–465

[2] Danisch S, Krumbiegel J (2021) Makie.jl: Flexible high-performance data visualization for Julia. Journal of Open Source Software 6(65):3349, DOI 10.21105/joss.03349, URL `https://doi.org/10.21105/joss.03349`

[3] Huang Y, Yan L, Yang T, Hu Z, Xu W (2023) Sensing design, trajectory planning, and motion control of a cable-driven redundant manipulator composed of quaternion joints. Journal of Mechanisms and Robotics 15(5):055001

[4] John I, Mohan S, Wenger P (2024) Kinetostatic analysis of a spatial cable-actuated variable stiffness joint. Journal of Mechanisms and Robotics 16(9)

[5] Kim YJ, Kim JI, Jang W (2018) Quaternion joint: Dexterous 3-dof joint representing quaternion motion for high-speed safe interaction. In: 2018 IEEE/RSJ international conference on intelligent robots and systems (IROS), IEEE, pp 935–942

[6] Liu F, Huang H, Li B, Hu Y, Jin H (2020) Design and analysis of a cable-driven rigid–flexible coupling parallel mechanism with variable stiffness. Mechanism and Machine Theory 153:104030

[7] Muralidharan V, Wenger P (2021) Optimal design and comparative study of two antagonistically actuated tensegrity joints. Mechanism and Machine Theory 159:104249

[1] https://drive.google.com/file/d/193kAAod791jivvCuxTmaF3dUG5zR1slv/view?usp=sharing

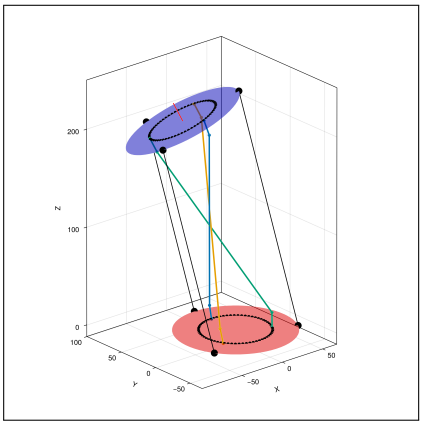

(a) Feasible solution when $(\theta,\ \psi) = (-20°,\ -18°)$

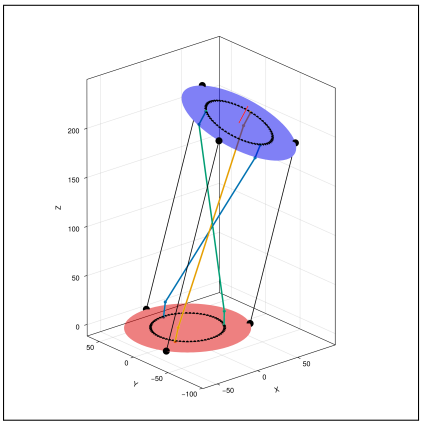

(b) Feasible solution when $(\theta,\ \psi) = (20°,\ 17°)$

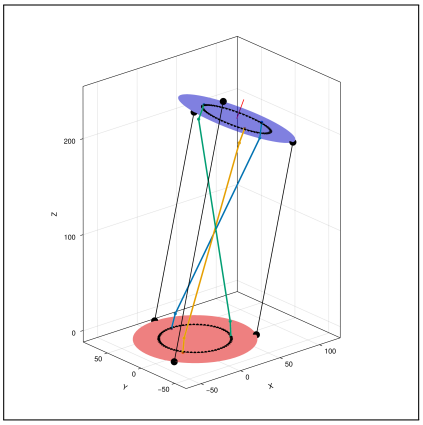

(c) Feasible solution when $(\theta,\ \psi) = (-13°,\ 37°)$

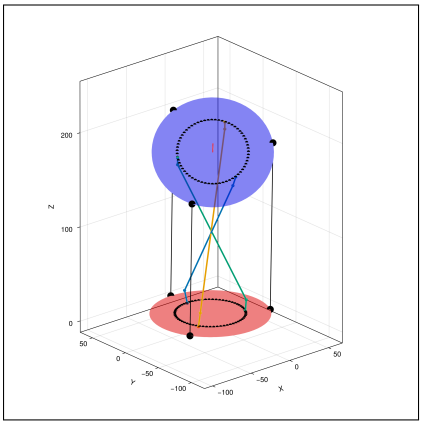

(d) Feasible solution when $(\theta,\ \psi) = (34°,\ -25°)$

Fig. 2: Feasible IK solutions at various platform poses $(\theta,\ \psi)$. The three cables are depicted as black solid lines. The images are generated using the Makie package [2] in Julia.

[8] Muralidharan V, Wenger P, Chevallereau C (2024) Optimal design and comparison of 2-x and 2-r planar cable-driven tensegrity-inspired manipulators. Mechanism and Machine Theory 200:105721

[9] Muñoz K, Porez M, Wenger P (2024) Kinematic and static analyses of a 3-dof spatial tensegrity mechanism. In: Lenarčič J, Husty M (eds) Advances in Robot Kinematics 2024, Springer, Springer Proceedings in Advanced Robotics, vol 31, p 36, DOI 10.1007/978-3-031-64057-5_36